Cloudy sky contributions to the direct aerosol effect

Gunnar Myhre[1], Bjørn H. Samset[1], Christian W. Mohr[1], Kari Alterskjær[1], Yves Balkanski[2], Nicholas Bellouin[3], Mian Chin[4], James Haywood[5,6], Øivind Hodnebrog[1], Stefan Kinne[7], Guangxing Lin[8,9], Marianne T. Lund[1], Joyce. E. Penner[10], Michael Schulz[11], Nick Schutgens[12], Ragnhild B. Skeie[1], Philip Stier[13], Toshihiko Takemura[14], Kai Zhang[15]

[1]CICERO Center for International Climate Research, Oslo, Norway.
[2]Laboratoire des Sciences du Climat et de l'Environnement, CEA-CNRS-UVSQ-UPSaclay, Gif-sur-Yvette, France.
[3]Department of Meteorology, University of Reading, Reading, RG6 6BB, UK.
[4]NASA Goddard Space Flight Center, Greenbelt, MD 20771 USA.
[5]College of Engineering, Mathematics and Physical Sciences, University of Exeter, Exeter, EX4 4QF, UK
[6]Earth System and Mitigation Science, Met Office Hadley Centre, Exeter, EX1 3PB, UK
[7]Max Plank Institute for Meteorology, Hamburg, Germany.
[8]University of Michigan, Ann Arbor, MI, USA.
[9]now at Atmospheric Sciences and Global Change Division, Pacific Northwest National Laboratory, Richland, WA, USA
[10]Department of Climate and Space Sciences and Engineering, University of Michigan, U. S. A
[11]Norwegian Meteorological Institute, Oslo, Norway.
[12]Earth Sciences, Faculty of Science, Vrije Universiteit Amsterdam, Amsterdam, Netherlands.
[13]Atmospheric, Oceanic and Planetary Physics, Department of Physics, University of Oxford, UK
[14]Research Institute for Applied Mechanics, Kyushu University, Fukuoka, Japan.
[15]Pacific Northwest National Laboratory, Richland, WA, USA

Corresponding author: Gunnar Myhre (gunnar.myhre@cicero.oslo.no)

Abstract: The radiative forcing of the aerosol-radiation interaction can be decomposed into clear sky and cloudy sky portions. Two sets of multi-model simulations within AeroCom, combined with observational methods, and the time evolution of aerosol emissions over the industrial era show that the contribution from cloudy sky regions is likely weak. A mean of the simulations considered is 0.01 ± 0.1 Wm^{-2}. Multivariate data analysis of results from AeroCom Phase II shows that many factors influence the strength of the cloudy sky contribution to the forcing of the aerosol-radiation interaction. Overall, single scattering albedo of anthropogenic aerosols and the interaction of aerosols with the shortwave cloud radiative effects are found to be important factors. A more dedicated focus on the contribution from the cloud free and cloud covered sky fraction respectively to the aerosol-radiation interaction will benefit the quantification of the radiative forcing and its uncertainty range.

1 Introduction

The radiative forcing (RF) of anthropogenic aerosols in the atmosphere due to the aerosol-radiation interaction – RFari (earlier denoted as direct aerosol effect) was assessed as -0.35 [-0.85 to +0.15] Wm^{-2} in the Fifth Assessment Report by the Intergovernmental Panel on Climate Chang (IPCC) (AR5) (Boucher et al., 2013). The AR5 uncertainty range is even slightly wider than in the Fourth Assessment Report (Forster et al., 2007). Despite major progress in the understanding of atmospheric aerosol composition, and almost two decades of multi-aerosol type model simulations, little progress had been made in reducing the large uncertainty in this number, until recently where Bellouin et al. (2020) estimate a range of -0.45 to -0.05 Wm^{-2}. Bellouin et al. estimate RFari from normalized clear sky radiative effect by aerosol optical depth (AOD) and multiply this by an assessment of anthropogenic AOD. No direct simulations were used to calculate the RFari in regions of clouds.

One reason for the larger uncertainty range in AR5 compared to AR4 was enhanced uncertainty and magnitude of the RFari of black carbon (BC) (Boucher et al., 2013). Bond et al. (2013) indicated that emission of BC was too low in the inventories applied in climate models and therefore scaled the RFari from models to observed Aeronet absorption aerosol optical depth (AAOD) retrievals. More recently it has been suggested that AAOD data from Aeronet may have a sampling bias due to sites being located close to emission source regions (Wang et al., 2018), but uncertain in magnitude (Schutgens, 2019) and that most global aerosol models may have a bias towards too much BC in the middle and upper troposphere (Kipling et al., 2013; Samset et al., 2014; Wang et al., 2014). Both of these factors indicate a too strong BC RFari in Bond et al. (2013). However, the most recent estimates of emission from fossil and biofuel BC (Hoesly et al., 2018) is much higher than used in previous global modelling (Lamarque et al., 2010). These new findings indicate that the BC RFari may be stronger than what was given in some of the multi-model global aerosol modelling exercises (Myhre et al., 2013a; Schulz et al., 2006), but likely weaker than estimated in Bond et al. (2013). The uncertainties in the RFari are also large for other aerosol species. For nitrate (Bian et al., 2017) the abundance is particularly uncertain, and for organic aerosols uncertainties are large both due to abundance (Tsigaridis et al., 2014) and the optical properties, particularly for brown carbon (Samset et al., 2018).

A further complication when estimating RFari is the atmospheric mix of scattering and absorbing aerosols. Since RFari is dependent on aerosol optical properties and the underlying albedo (Haywood and Shine, 1997), it is therefore also very dependent on where the aerosols are located relative to clouds (Takemura et al., 2002). Absorbing aerosols above clouds have a strong positive RFari (Chand et al., 2009; Keil and Haywood, 2003) but it becomes considerably weaker if the aerosols are located below clouds (Takemura et al., 2002). Scattering aerosols above or below clouds may enhance the reflection of solar radiation in conditions of thin clouds. The all sky RFari can be separated into contributions from clear and cloudy sky portions:

$$\mathbf{RFari}_{\mathbf{all\ sky}} = \mathbf{RFari}_{\mathbf{clear}} + \mathbf{RFari}_{\mathbf{cloud}} \quad (1)$$

$RFari_{clear}$ and $RFari_{cloud}$ are the clear sky and cloudy sky portion to $RFari_{allsky}$, respectively. $RFari_{clear}$ and $RFari_{cloud}$ can further be described as $RFari_{clear} = (1\text{-}AC) * RFari_{total\text{-}clear}$ and $RFari_{cloud} = AC * RFari_{ctotal\text{-}cloud}$, where AC is cloud fraction, $RFari_{total\text{-}clear}$ is simulations excluding all clouds and $RFari_{total\text{-}cloud}$ is the aerosol radiative effect assuming the whole grid is covered by

clouds. All three variables vary as a function of longitude, latitude and time. The RFari is the initial perturbation to top of the atmosphere (TOA) radiative fluxes (the instantaneous RF which for aerosol is very similar to RF). Rapid adjustments from shortwave absorption by aerosols, mostly BC, may alter atmospheric temperatures, water vapour and clouds. The sum of RFari and rapid adjustments is denoted effective radiative forcing (Boucher et al., 2013; Myhre et al., 2013b; Sherwood et al., 2015). The rapid adjustment of absorbing aerosols can be strong and may counteract the RFari substantially (Smith et al., 2018). Since RFari includes no rapid adjustments, AC is constant in simulations of $RFari_{clear}$ and $RFari_{cloud}$. Oikawa et al. (2013); Oikawa et al. (2018) provide estimates of all sky, clear sky and cloudy sky radiative effect of aerosols in different regions based on satellite retrievals of clouds and aerosols. These studies further describe large differences resulting from whether aerosols are below or above clouds. Lacagnina et al. (2017); Zhang et al. (2016) found large regional variation in the radiative effect of aerosols above clouds. Note that the above-mentioned studies investigate the present, total aerosol abundance which consist of anthropogenic and natural aerosols, whereas in terms of RFari only the anthropogenic aerosols are considered. Anthropogenic aerosols are changes to the atmospheric composition since pre-industrial time. Matus et al. (2019) combined satellite derived aerosol radiative effect with model simulation of anthropogenic aerosol, to make an estimate of RFari.

The aim of the present study is to provide insight into factors determining $RFari_{cloud}$ and thus the contribution from cloudy sky regions to the RFari from combining global models and observational based approaches. We present estimates of this quantity from several global studies and we use multivariate data analysis to provide insight on the core factors causing the diversity among models.

2 Methods

2.1 Global estimates of cloudy sky contribution to RFari

The models, experiments and RFari from AeroCom Phase I and II are documented in detail by Schulz et al. (2006) and Myhre et al. (2013a), respectively. We also analyze the historical evolution of RFari due to anthropogenic aerosols using output from a series of OsloCTM3 simulations (Lund et al., 2018) with emissions from the Community Emission Data System (CEDS) (Hoesly et al., 2018) inventory from year 1750 to 2014. The OsloCTM3 is a global 3-dimensional chemistry-transport model driven by 3-hourly meteorological forecast data.

The analysis is further supplemented by variables from Equation 1 extracted from Myhre (2009), who presented results from OsloCTM2 and an observational based method to explain the difference in all sky RFari between observational based and global aerosol model approaches. The model simulations were made to investigate several assumptions on aerosol optical properties and impacts of assumptions related to missing data and change in industrial era aerosol concentration for the observational method. The Max Planck Aerosol Climatology (MACv2) method combines aerosol column optical properties for fine-mode and coarse-mode sizes (of an AeroCom phase1 model median

regionally adjusted by AERONET/MAN monthly statistics) with MODIS surface albedo data, ISCCP cloud properties and vertical scaling by size-mode from 20 years of ECHAM-HAM aerosol simulations. The anthropogenic properties is defined as a fraction of the fine-mode, where the fine-mode AOD scaling factor prescribed from AeroCom phase1 simulations. (Kinne, 2019a; Kinne, 2019b).

The cloudy sky contribution to all sky RFari is calculated from daily or monthly diagnostics of allsky RFari, $RFari_{clear}$ and AC. RF is taken at the top of the atmosphere and all estimates are from pre-industrial to present.

2.2 Multivariate data analysis

Multivariate data analysis in this study is based on results from a subset of the models participating in AeroCom Phase II (CAM5, GOCART, HadGEM2, IMPACT, INCA, ECHAM-HAM, OsloCTM2 and SPRINTARS). These eight models participated in the AeroCom Phase II experiment (Myhre et al., 2013a) with no constrain on aerosol processes and in addition participated in the host model AeroCom exercise with fixed aerosol optical properties (Stier et al., 2013). From the latter FIX2scat and FIX3abs experiments can be used to retrieve the contributions from cloudy sky to RFari in two highly idealized aerosol radiative properties experiments. FIX2scat is a purely scattering aerosol case and FIX3abs is an absorbing aerosol case. The origin of the different variables derived from AeroCom phase II model simulations (Myhre et al., 2013a; Samset et al., 2013) can be found Table 1.

The global mean data in Table 1 is analyzed using principal component analysis (PCA). Here, the variables that may influence the $RFari_{cloud}$ are orthogonally transformed into linearly uncorrelated variables named principal components (PCs). The transformation is defined so that the first principal component (PC1) accounts for most of variance exhibited by the underlying variables. PCA is a dimension reduction technique, allowing for the visualization of all the variance between the variables in a two-dimensional plot (biplot). All PCs are anticorrelated with each other, which is why PC1 and PC2 are perpendicular to each other. How the variables relate to each other can to some extent be explained (magnitude) with each exceeding PC. In other words, each PC does not exclusively show its relation to $RFari_{cloud}$.

Data is normalized prior to PCA to ensure comparison of variance between variables. PCA results are usually plotted in a biplot, where only PC1 and PC2 (the second PC) are plotted on the x- and y-axis, respectively, since the two PCs explain most of the variance. In the biplot variables are projected as vectors along PC1 and PC2. The combined length and direction of the vector indicates the correlation the variable has with PC1 and PC2. Values range from -1 to 1 indicating negative to positive correlation with the PC. A value of 0 indicates no correlation with the PC. Since the projected vectors are directional it is possible to have high correlation with PC1 (values ~ -1 or ~ 1), and poor correlation with PC2 (value ~ 0), or *visa-versa*. Variables that point in the same direction are positively correlated with each other. Variables that point in the opposite direction of each other are negatively correlated. Variables that are perpendicular to each other are not correlated with each other. The missing data (see Table 1) for two of the models (LMDZ-INCA and ECHAM-HAM) are filled-in using regularized iterative

PCA. This technique estimates the missing values, based on the correlation between the variables and the principal components (Josse and Husson, 2012).

The $RFari_{cloud}$ (second term in Equation 1) is added as a supplementary variable in the PCA. This is to ensure that this dependent variable, the cloudy sky contribution, does not influence the projected correlations the independent variables have on each other. The same approach is applied to FIX2scat and FIX3abs, as these variables are not independent, as they are composed of the many of the variables used in the analysis. In addition, linear regression correlation coefficients are calculated between all the variables to assess the individual relationships.

3 Results

3.1 Estimates of cloudy sky contributions to RFari

Figure 1 shows the all sky RFari due to anthropogenic aerosols separated into clear sky (first term on right-hand side in equation 1) and cloudy sky (second term on right-hand side in equation 1) portion from AeroCom Phase II models (Myhre et al., 2013a). The uncertainty ranges given in the figure are one standard deviation among the global aerosol models in AeroCom Phase II. The figure shows two main results, that the cloudy sky RFari is weak and that the uncertainties in the contributions from cloudy sky and clear sky are substantial with the latter somewhat larger in magnitude.

Figure 2 shows an example from OsloCTM3 (Lund et al., 2018) of the spatial distribution terms involved in equation 1. In the lower row of Figure 2 the annual mean AC, $RFari_{clear\text{-}total}$ and $RFari_{cloud\text{-}total}$ are shown, with strong negative $RFari_{clear\text{-}total\text{-}}$ over most land areas except over regions of high surface albedo such as deserts. The $RFari_{cloud\text{-}total}$ is particularly positive over regions of biomass burning aerosols overlying low level stratocumulus, but also over parts of high aerosol abundance over China. The second row shows the two terms on the right hand in equation 1, namely the contribution from the cloud free and cloudy regions to the all sky RFari. The contribution from the clear sky regions ($RFari_{clear}$, first term on the right-hand side of equation 1) is much weaker than $RFari_{clear\text{-}total}$ itself since cloud fraction is high in many of the regions of anthropogenic aerosols. While the influence from cloud fraction on $RFari_{cloud}$ relative to $RFari_{cloud\text{-}total}$ is weak over biomass burning regions, it weakens relative to the negative values in $RFari_{cloud\text{-}total}$ over many areas in the northern hemisphere. In the top row the RFari all sky is the sum of the contributions from clear and cloudy regions where their importance for the RFari varies regionally.

Figure 3a-d shows estimates of the contribution from cloud sky to RFari from several studies: two are multi-model studies, one combines model and observational based methods and one study investigates the time evolution using one model. The two multi-model AeroCom studies (Myhre et al., 2013a; Schulz et al., 2006) show that the sign varies among the global aerosol models and that two versions from one model changes sign between the two AeroCom phases (two versions of ECHAM-HAM, UIOCTM versus OsloCTM2, and UMI versus IMPACT). The two model versions INCA and LSCE have positive values in both AeroCom phases. SPRINTARS has the strongest positive (and overall strongest magnitude) $RFari_{cloud}$ in both

AeroCom phases. About half of the models shown in Figure 3a and 3b have provided sufficient diagnostics to extract estimates from both AeroCom phases. The AeroCom PhaseII results will be further discussed in section 3.2.

In Myhre (2009) several experiments were performed to explain that differences in RFari between observational based methods and global aerosol models arise from a relatively larger change in absorbing aerosols over the industrial era than in the current abundance of the absorbing aerosols. Whereas an observational method uses aerosol optical properties from measurements of the present time of the combined natural and anthropogenic aerosols, the models simulate a relatively larger change in the abundance of anthropogenic absorbing aerosols than assuming no change in the industrial era aerosol optical properties. Figure 3c shows the contribution of the cloudy sky to RFari from several of these experiments. The two experiments MODIS(SCREEN) and MODIS use satellite retrievals of aerosol optical depth (AOD), present aerosol optical properties retrieved (single scattering albedo and asymmetry factor) from AERONET, and a model estimate of the anthropogenic AOD. The difference between these experiments is that the MODIS experiment uses model information over regions of missing AOD from the satellite retrievals, while these regions are ignored in MODIS(SCREEN). $RFari_{cloud}$ is similar in these two experiments. On the other hand, in the experiment MODIS(Model), changes in the aerosol optical properties from pre-industrial to present causes the change in sign in the cloud sky contribution to RFari compared to MODIS and MODIS(SCREEN). The MODIS(Model) has very similar RFari, as well as $RFari_{cloud}$, to the standard global aerosol model simulations (MODEL INT and MODEL EXT). The two latter model simulations differ on whether internal or external mixing of BC is taken into account, respectively. The MACv2 $RFari_{cloud}$ is -0.13 Wm^{-2}. This estimate does not consider change in the aerosol optical properties over the industrial era and can thus be compared to MODIS(SCREEN) and MODIS experiments described above.

The time evolution of the contribution of cloudy sky to RFari in OsloCTM3 is shown in Figure 3d where all variations are caused by changes in the anthropogenic aerosol composition and abundance since all other factors are kept constant. Values are negative in the period 1960 to 1990 due to a strong increase in SO_2 emissions and thereby a domination of scattering aerosols and radiative impacts even in cloudy skies. In the period after 1990 the regional SO_2 emissions have changed strongly, but with a small reduction in the global emissions. Emissions of BC have on the other hand increased substantially making anthropogenic aerosols more absorbing in the OsloCTM3 causing a relatively stronger positive contribution from the cloudy sky to RFari.

3.2 Multivariate data analysis of cloudy sky contribution to the all sky RFari

Table 1 lists the AeroCom Phase II models and variables included in the multivariate data analysis for investigating $RFari_{cloud}$ denoted as "Cloudy" in the table (the second term on the right-hand side of equation 1). The results of the multivariate data analysis are plotted in a biplot and a correlogram Figure 4. The principal component analysis (PCA) found that 68.2% of the total variance is explained by the first and second principal component (PC1 and PC2), see Figure 4a. Adding PC3 this number increases to 89.2% (see Figure 4c). The analysis shows that several factors are important for the contribution of cloudy sky to

RFari ("Cloudy"). Among all variables total short-wave cloud radiative effect (SW_CRE) is the most important. SW_CRE is near perfectly positively correlated with PC2 (Figure 4a), hence it must be anticorrelated with every other PCs. Therefore, the vector in Figure 4a is perpendicular to the PC1 axis. This is also why the length of the vector is so short in Figure 4c since it neither correlates with PC3 nor PC1. SW_CRE is correlated with PC2 and Cloudy is correlated with PC2. The vector is pointing in the opposite direction between SW_CRE and Cloudy, which means the two variables are negatively correlated with each other. Figure 4b also shows a negative correlation between the two variables. A biplot with PC1 and PC3 (Figure 4c) can explain more about a variable than PC1 and PC2. For example, CL_ALT has a slightly stronger projection in the PC1 and PC3 biplot and suggest that there is an anticorrelation with FIX2scat. However, in the PC1 and PC2 they are positively correlated with each other. This suggest that there is partial correlation and Figure 4b shows there is a weak positive correlation between these two variables.

Single scattering albedo (SSA) being a crucial variable for the anthropogenic aerosols may potentially be an important factor (a higher SSA is expected to give a more negative cloudy sky forcing). However, independent correlations plotted in the correlogram (Figure 4b) suggests that the contribution to $RFari_{cloud}$ and SSA is weak ($r = 0.17$). In depth analysis of the linear correlation between cloudy sky to RFari and SSA suggests that the linear relationship exist only at higher PCs (see Figure 4c). The contribution of cloudy sky to RFari shows a closer dependence on similar quantities for the idealized experiment FIX3abs than FIX2scat, where FIX2scat has purely scattering aerosols. Both FIX2scat and FIX3abs are dependent on host model properties such as surface albedo and radiative transfer schemes (Stier et al., 2013). They are further strongly dependent on the host model clouds and their radiative effect and anticorrelated to cloud fraction (CLD_FR) and SW_CRE, respectively.

PCA finds negative correlation between $RFari_{cloud}$ and total short-wave cloud radiative flux (SW_CRE), also supported by the linear regression. One example here is the GOCART model with the weakest SW_CRE and most negative cloudy sky contribution to RFari of the models included in the multivariate data analysis. At the same time the PCA finds a small dependence between the cloudy sky contribution to RFari and cloud fraction (CLD_FR) or cloud altitude (CL_ALT). The negative correlation between $RFari_{cloud}$ and SW_CRE can be explained by reflective clouds enhancing the underlying albedo and thus making the radiative forcing more positive with an increase in absorbing aerosols in the cloudy sky portion.

Overall FIX3abs (where models have a fixed SSA) and SW_CRE seem to be the main explanatory variables for the variance in the cloudy sky contribution to RFari. It is however worth noting that the correlation for cloudy sky contribution to RFari with the variables is not particular strong in any direction (indicated by the short arrow). This suggests that some of the variance may be explained along the third or fourth principal component etc.

4 Discussion and conclusions

The multivariate data analysis shows that host model characteristics (especially SW_CRE) are important for the modelled cloudy sky contribution to RFari ($RFari_{cloud}$), but further indicates that many other factors are important. Furthermore, several

other studies presented here show that aerosol properties (in particular SSA) are important for this quantity. Locally and especially in regions with aerosols above clouds, as well as in single model studies the SSA is crucial for $RFari_{cloud}$. The two AeroCom phases give $RFari_{cloud}$ estimates of 0.0 ± 0.10 Wm^{-2} and 0.04 ± 0.10 Wm^{-2} and the mean of two observational based methods is -0.02 (range from -0.13 to 0.09 Wm^{-2}). Combining the numbers from these three studies, we find a $RFari_{cloud}$ of 0.01 ± 0.1 Wm^{-2}. The new emission inventory from CEDS has a strong increase in BC emissions leading to an increase in $RFari_{cloud}$of 0.05 Wm^{-2} from 2000 to 2014 in OsloCTM3. Using OsloCTM3 simulations to investigate the importance of diagnostics for every radiation time step (3 hourly) shows differences up to 0.01 W m^{-2} relative to daily mean data and up to 0.04 W m^{-2} for monthly data, but this may be model dependent (Haywood and Shine, 1997). The simulations used in this study only include the RF of the aerosol-radiation interaction. In a recent multi-model study, a decomposition of all aerosol effect (including aerosol-cloud interactions) provides weak $RFari_{cloud}$ for all models, of magnitude and multi-model mean similar to this study (Gryspeerdt et al., 2020). A separate single-model study however found $RFari_{cloud}$ to be substantial (Ghan, 2013).

Determining the quantity of black carbon from instrumentation such as the SP2 has provided a new set of consistent data for assessing the performance of aerosol models (e.g. Kipling et al. (2013); Wang et al. (2014)). Knowledge of BC mass is fundamentally insufficient for determining the ambient aerosol single scattering albedo owing to additional complexities such as the degree of internal and external mixing. In the past, the aerosol modelling community has relied either on indirect remotely sensed measurements from AERONET (e.g. Chin et al. (2009)) or on imperfect in-situ measurements of aerosol scattering from nephelometers (e.g. Anderson et al. (2003)) and absorption from filter-based systems (e.g. Bond et al. (1999)). Both of these systems are relatively imprecise corrections to account for scattering and absorption artifacts (e.g. Davies et al. (2019); Massoli et al. (2009)). The single scattering albedos can be determined much more accurately using combinations of cavity ring-down measurements of extinction (e.g. Lack et al. (2006)) and photoacoustic measurements of aerosol absorption (e.g. Baynard et al. (2006)). These instruments are becoming more routine on aircraft equipped for making atmospheric measurements that can make highly accurate assessments of the aerosol single scattering albedo at above-cloud altitudes (e.g. Davies et al. (2019); Langridge et al. (2011)). These measurements will provide an invaluable additional source of data for model evaluation. All the global models that supplied simulations for this study treat the major anthropogenic aerosol components sulphate, organic aerosols, and black carbon, some also treat nitrate, but none include anthropogenic dust aerosols which have highly uncertain radiative effects.

Koffi et al. (2016); Koffi et al. (2012) show that global aerosol models generally tend to have an overabundance of aerosols at higher altitude compared to satellite retrievals from CALIPSO and Samset et al. (2014) show that the AeroCom models overestimate BC at mid and high tropospheric altitudes compared to aircraft measurements. Too much BC above the clouds would overestimate $RFari_{cloud}$. On the other hand, Peers et al. (2016) show that over the biomass burning region in south Africa most of the AeroCom models underestimate the AAOD over the stratocumulus layer, which would underestimate $RFari_{cloud}$.

In future studies of RFari, particular attention should be put on how global aerosol models simulate the location of aerosols in relation to clouds and how aerosol optical properties change with altitude in regions with high cloud cover compared to measurements in order to further constrain the spread in the modelled cloudy sky contribution. Nowhere is this high sensitivity more clearly demonstrated than over the SE Atlantic where biomass burning aerosols over-lie (and sometimes interact with) relatively bright stratocumulus clouds (e.g. Zuidema et al. (2016)). In addition to further analysis of aerosol RF in cloudy sky regions, more emphasis should be devoted to quantifying the RFari in cloud free regions and its trend (Paulot et al., 2018), where the magnitude of forcing is larger than in cloudy regions.

Acknowledgments, Samples, and Data

All AeroCom data are available at the AeroCom server (https://aerocom.met.no/). The OsloCTM data will be made available through NIRD Research Data Archive. GM received funding from the Research Council of Norway through the SUPER (grant 250573). PS was supported by the European Research Council (ERC) project constRaining the EffeCts of Aerosols on Precipitation (RECAP) under the European Union's Horizon 2020 research and innovation programme with grant agreement No 724602.

References

Anderson, T. L., Masonis, S. J., Covert, D. S., Ahlquist, N. C., Howell, S. G., Clarke, A. D. and McNaughton, C. S.: Variability of aerosol optical properties derived from in situ aircraft measurements during ACE-Asia, Journal of Geophysical Research: Atmospheres, 108(D23), 2003.

Baynard, T., Garland, R. M., Ravishankara, A. R., Tolbert, M. A. and Lovejoy, E. R.: Key factors influencing the relative humidity dependence of aerosol light scattering, Geophysical Research Letters, 33(6), 2006.

Bellouin, N., Quaas, J., Gryspeerdt, E., Kinne, S., Stier, P., Watson-Parris, D., Boucher, O., Carslaw, K. S., Christensen, M., Daniau, A.-L., Dufresne, J.-L., Feingold, G., Fiedler, S., Forster, P., Gettelman, A., Haywood, J. M., Lohmann, U., Malavelle, F., Mauritsen, T., McCoy, D. T., Myhre, G., Mülmenstädt, J., Neubauer, D., Possner, A., Rugenstein, M., Sato, Y., Schulz, M., Schwartz, S. E., Sourdeval, O., Storelvmo, T., Toll, V., Winker, D. and Stevens, B.: Bounding Global Aerosol Radiative Forcing of Climate Change, Reviews of Geophysics, 58(1), e2019RG000660, 2020.

Bian, H., Chin, M., Hauglustaine, D. A., Schulz, M., Myhre, G., Bauer, S. E., Lund, M. T., Karydis, V. A., Kucsera, T. L., Pan, X., Pozzer, A., Skeie, R. B., Steenrod, S. D., Sudo, K., Tsigaridis, K., Tsimpidi, A. P. and Tsyro, S. G.: Investigation of global particulate nitrate from the AeroCom phase III experiment, Atmos. Chem. Phys., 17, 12911-12940, 2017.

Bond, T. C., Anderson, T. L. and Campbell, D.: Calibration and Intercomparison of Filter-Based Measurements of Visible Light Absorption by Aerosols, Aerosol Science and Technology, 30(6), 582-600, 1999.

Bond, T. C., Doherty, S. J., Fahey, D. W., Forster, P. M., Berntsen, T., DeAngelo, B. J., Flanner, M. G., Ghan, S., Karcher, B., Koch, D., Kinne, S., Kondo, Y., Quinn, P. K., Sarofim, M. C., Schultz, M. G., Schulz, M., Venkataraman, C., Zhang, H., Zhang, S., Bellouin, N., Guttikunda, S. K., Hopke, P. K., Jacobson, M. Z., Kaiser, J. W., Klimont, Z., Lohmann, U., Schwarz, J. P., Shindell, D., Storelvmo, T., Warren, S. G. and Zender, C. S.: Bounding the role of black carbon in the climate system: A scientific assessment, Journal of Geophysical Research-Atmospheres, 118(11), 5380-5552, 2013.

Boucher, O., Randall, D., Artaxo, P., Bretherton, C., Feingold, G., Forster, P., Kerminen, V.-M., Kondo, Y., Liao, H., Lohmann, U., Rasch, P., Satheesh, S. K., Sherwood, S., Stevens, B. and Zhang, X.-Y., Clouds and Aerosols. In: Climate Change 2013: The Physical Science Basis. Contribution of Working Group I to the Fifth Assessment Report of the Intergovernmental Panel on Climate Change. T. F. Stocker, D. Qin, G.-K. Plattner, M. Tignor, S. K. Allen et al. (Editors), Cambridge University Press, Cambridge, United Kingdom and New York, NY, USA, pp. 571-657, 2013.

Chand, D., Wood, R., Anderson, T. L., Satheesh, S. K. and Charlson, R. J.: Satellite-derived direct radiative effect of aerosols dependent on cloud cover, Nature Geoscience, 2(3), 181-184, 2009.

Chin, M., Diehl, T., Dubovik, O., Eck, T. F., Holben, B. N., Sinyuk, A. and Streets, D. G.: Light absorption by pollution, dust, and biomass burning aerosols: a global model study and evaluation with AERONET measurements, Annales Geophysicae, 27(9), 3439-3464, 2009.

Davies, N. W., Fox, C., Szpek, K., Cotterell, M. I., Taylor, J. W., Allan, J. D., Williams, P. I., Trembath, J., Haywood, J. M. and Langridge, J. M.: Evaluating biases in filter-based aerosol absorption measurements using photoacoustic spectroscopy, Atmos. Meas. Tech., 12(6), 3417-3434, 2019.

Forster, P., Ramaswamy, V., Artaxo, P., Berntsen, T., Betts, R., Fahey, D. W., Haywood, J., Lean, J., Lowe, D. C., Myhre, G., Nganga, J., Prinn, R., Raga, G., Schulz, M. and Van Dorland, R., Changes in Atmospheric Constituents and in Radiative Forcing. In: Climate Change 2007: The Physical Science Basis. Contribution of Working Group I to the Fourth Assessment Report of the Intergovernmental Panel on Climate Change, Cambridge University Press, Cambridge, United Kingdom and New York, NY, USA, 2007.

Ghan, S. J.: Technical Note: Estimating aerosol effects on cloud radiative forcing, Atmospheric Chemistry and Physics, 13(19), 9971-9974, 2013.

Gryspeerdt, E., Mülmenstädt, J., Gettelman, A., Malavelle, F. F., Morrison, H., Neubauer, D., Partridge, D. G., Stier, P., Takemura, T., Wang, H., Wang, M. and Zhang, K.: Surprising similarities in model and observational aerosol radiative forcing estimates, Atmos. Chem. Phys., 20(1), 613-623, 2020.

Haywood, J. M. and Shine, K. P.: Multi-spectral calculations of the direct radiative forcing of tropospheric sulphate and soot aerosols using a column model, Quarterly Journal of the Royal Meteorological Society, 123(543), 1907-1930, 1997.

Hoesly, R. M., Smith, S. J., Feng, L., Klimont, Z., Janssens-Maenhout, G., Pitkanen, T., Seibert, J. J., Vu, L., Andres, R. J., Bolt, R. M., Bond, T. C., Dawidowski, L., Kholod, N., Kurokawa, J. I., Li, M., Liu, L., Lu, Z., Moura, M. C. P., O'Rourke, P. R. and Zhang, Q.: Historical (1750–2014) anthropogenic emissions of reactive gases and aerosols from the Community Emissions Data System (CEDS), Geosci. Model Dev., 11(1), 369-408, 2018.

Josse, J. and Husson, F.: Handling missing values in exloratory multivariate data analysis methods, Journal de la Société Fraçaise de Statistique, 153, 79–99, 2012.

Keil, A. and Haywood, J. M.: Solar radiative forcing by biomass burning aerosol particles during SAFARI 2000: A case study based on measured aerosol and cloud properties, Journal of Geophysical Research-Atmospheres, 108(D13), 8467, 2003.

Kinne, S.: Aerosol radiative effects with MACv2, Atmos. Chem. Phys., 19(16), 10919-10959, 2019a.

Kinne, S.: The MACv2 aerosol climatology, Tellus B: Chemical and Physical Meteorology, 71(1), 1-21, 2019b.

Kipling, Z., Stier, P., Schwarz, J. P., Perring, A. E., Spackman, J. R., Mann, G. W., Johnson, C. E. and Telford, P. J.: Constraints on aerosol processes in climate models from vertically-resolved aircraft observations of black carbon, Atmos. Chem. Phys., 13(12), 5969-5986, 2013.

Koffi, B., Schulz, M., Bréon, F.-M., Dentener, F., Steensen, B. M., Griesfeller, J., Winker, D., Balkanski, Y., Bauer, S. E., Bellouin, N., Berntsen, T., Bian, H., Chin, M., Diehl, T., Easter, R., Ghan, S., Hauglustaine, D. A., Iversen, T., Kirkevåg, A., Liu, X., Lohmann, U., Myhre, G., Rasch, P., Seland, Ø., Skeie, R. B., Steenrod, S. D., Stier, P., Tackett, J., Takemura, T., Tsigaridis, K., Vuolo, M. R., Yoon, J. and Zhang, K.: Evaluation of the aerosol vertical distribution in global aerosol models through comparison against CALIOP measurements: AeroCom phase II results, Journal of Geophysical Research: Atmospheres, 121(12), 7254-7283, 2016.

Koffi, B., Schulz, M., Breon, F. M., Griesfeller, J., Winker, D., Balkanski, Y., Bauer, S., Berntsen, T., Chin, M. A., Collins, W. D., Dentener, F., Diehl, T., Easter, R., Ghan, S., Ginoux, P., Gong, S. L., Horowitz, L. W., Iversen, T., Kirkevag, A., Koch, D., Krol, M., Myhre, G., Stier, P. and Takemura, T.: Application of the CALIOP layer product to evaluate the vertical distribution of aerosols estimated by global models: AeroCom phase I results, Journal of Geophysical Research-Atmospheres, 117, D10201, doi:10.1029/2011jd016858, 2012.

Lacagnina, C., Hasekamp, O. P. and Torres, O.: Direct radiative effect of aerosols based on PARASOL and OMI satellite observations, Journal of Geophysical Research: Atmospheres, 122(4), 2366-2388, 2017.

Lack, D. A., Lovejoy, E. R., Baynard, T., Pettersson, A. and Ravishankara, A. R.: Aerosol Absorption Measurement using Photoacoustic Spectroscopy: Sensitivity, Calibration, and Uncertainty Developments, Aerosol Science and Technology, 40(9), 697-708, 2006.

Lamarque, J., Bond, T., Eyring, V., Granier, C., Heil, A., Klimont, Z., Lee, D., Liousse, C., Mieville, A., Owen, B., Schultz, M., Shindell, D., Smith, S., Stehfest, E., Van Aardenne, J., Cooper, O., Kainuma, M., Mahowald, N., McConnell, J., Naik, V., Riahi, K. and van Vuuren, D.: Historical (1850-2000) gridded anthropogenic and biomass burning emissions of reactive gases and aerosols: methodology and application, Atmospheric Chemistry and Physics, 7017-7039, 2010.

Langridge, J. M., Richardson, M. S., Lack, D., Law, D. and Murphy, D. M.: Aircraft Instrument for Comprehensive Characterization of Aerosol Optical Properties, Part I: Wavelength-Dependent Optical Extinction and Its Relative Humidity Dependence Measured Using Cavity Ringdown Spectroscopy, Aerosol Science and Technology, 45(11), 1305-1318, 2011.

Lund, M. T., Myhre, G., Haslerud, A. S., Skeie, R. B., Griesfeller, J., Platt, S. M., Kumar, R., Myhre, C. L. and Schulz, M.: Concentrations and radiative forcing of anthropogenic aerosols from 1750 to 2014 simulated with the Oslo CTM3 and CEDS emission inventory, Geosci. Model Dev., 11(12), 4909-4931, 2018.

Massoli, P., Murphy, D. M., Lack, D. A., Baynard, T., Brock, C. A. and Lovejoy, E. R.: Uncertainty in Light Scattering Measurements by TSI Nephelometer: Results from Laboratory Studies and Implications for Ambient Measurements, Aerosol Science and Technology, 43(11), 1064-1074, 2009.

Matus, A. V., L'Ecuyer, T. S. and Henderson, D. S.: New Estimates of Aerosol Direct Radiative Effects and Forcing From A-Train Satellite Observations, Geophysical Research Letters, 46(14), 8338-8346, 2019.

Myhre, G.: Consistency between satellite-derived and modeled estimates of the direct aerosol effect, Science, 325(5937), 187-190, 2009.

Myhre, G., Samset, B. H., Schulz, M., Balkanski, Y., Bauer, S., Berntsen, T. K., Bian, H., Bellouin, N., Chin, M., Diehl, T., Easter, R. C., Feichter, J., Ghan, S. J., Hauglustaine, D., Iversen, T., Kinne, S., Kirkevag, A., Lamarque, J. F., Lin, G., Liu, X., Lund, M. T., Luo, G., Ma, X., van Noije, T., Penner, J. E., Rasch, P. J., Ruiz, A., Seland, O., Skeie, R. B., Stier, P., Takemura, T., Tsigaridis, K., Wang, P., Wang, Z., Xu, L., Yu, H., Yu, F., Yoon, J. H., Zhang, K., Zhang, H. and Zhou, C.: Radiative forcing of the direct aerosol effect from AeroCom Phase II simulations, Atmospheric Chemistry and Physics, 13(4), 1853-1877, 2013a.

Myhre, G., Shindell, D., Bréon, F.-M., Collins, W., Fuglestvedt, J., Huang, J., Koch, D., Lamarque, J.-F., Lee, D., Mendoza, B., Nakajima, T., Robock, A., Stephens, G., Takemura, T. and Zhang, H., Anthropogenic and Natural Radiative Forcing. In: Climate Change 2013: The Physical Science Basis. Contribution of Working Group I to the Fifth Assessment Report of the Intergovernmental Panel on Climate Change. T. F. Stocker, D. Qin, G.-K. Plattner, M. Tignor, S. K. Allen et al. (Editors), Cambridge University Press, Cambridge, United Kingdom and New York, NY, USA, pp. 659-740, 2013b.

Oikawa, E., Nakajima, T., Inoue, T. and Winker, D.: A study of the shortwave direct aerosol forcing using ESSP/CALIPSO observation and GCM simulation, Journal of Geophysical Research: Atmospheres, 118(9), 3687-3708, 2013.

Oikawa, E., Nakajima, T. and Winker, D.: An Evaluation of the Shortwave Direct Aerosol Radiative Forcing Using CALIOP and MODIS Observations, Journal of Geophysical Research: Atmospheres, 123(2), 1211-1233, 2018.

Paulot, F., Paynter, D., Ginoux, P., Naik, V. and Horowitz, L. W.: Changes in the aerosol direct radiative forcing from 2001 to 2015: observational constraints and regional mechanisms, Atmos. Chem. Phys., 18(17), 13265-13281, 2018.

Peers, F., Bellouin, N., Waquet, F., Ducos, F., Goloub, P., Mollard, J., Myhre, G., Skeie, R. B., Takemura, T., Tanré, D., Thieuleux, F. and Zhang, K.: Comparison of aerosol optical properties above clouds between POLDER and AeroCom models over the South East Atlantic Ocean during the fire season, Geophysical Research Letters, 43(8), 3991-4000, 2016.

Samset, B. H., Myhre, G., Herber, A., Kondo, Y., Li, S. M., Moteki, N., Koike, M., Oshima, N., Schwarz, J. P., Balkanski, Y., Bauer, S. E., Bellouin, N., Berntsen, T. K., Bian, H., Chin, M., Diehl, T., Easter, R. C., Ghan, S. J., Iversen, T., Kirkevåg, A., Lamarque, J. F., Lin, G., Liu, X., Penner, J. E., Schulz, M., Seland, Ø., Skeie, R. B., Stier, P., Takemura, T., Tsigaridis, K. and Zhang, K.: Modelled black carbon radiative forcing and atmospheric lifetime in AeroCom Phase II constrained by aircraft observations, Atmos. Chem. Phys., 14(22), 12465-12477, 2014.

Samset, B. H., Myhre, G., Schulz, M., Balkanski, Y., Bauer, S., Berntsen, T. K., Bian, H., Bellouin, N., Diehl, T., Easter, R. C., Ghan, S. J., Iversen, T., Kinne, S., Kirkevag, A., Lamarque, J. F., Lin, G., Liu, X., Penner, J. E., Seland, O., Skeie, R. B., Stier, P., Takemura, T., Tsigaridis, K. and Zhang, K.: Black carbon vertical profiles strongly affect its radiative forcing uncertainty, Atmospheric Chemistry and Physics, 13(5), 2423-2434, 2013.

Samset, B. H., Stjern, C. W., Andrews, E., Kahn, R. A., Myhre, G., Schulz, M. and Schuster, G. L.: Aerosol Absorption: Progress Towards Global and Regional Constraints, Current Climate Change Reports, 4(2), 65-83, 2018.

Schulz, M., Textor, C., Kinne, S., Balkanski, Y., Bauer, S., Berntsen, T., Berglen, T., Boucher, O., Dentener, F., Guibert, S., Isaksen, I. S. A., Iversen, T., Koch, D., Kirkevag, A., Liu, X., Montanaro, V., Myhre, G., Penner, J. E., Pitari, G., Reddy, S., Seland, O., Stier, P. and Takemura, T.: Radiative forcing by aerosols as derived from the AeroCom present-day and pre-industrial simulations, Atmospheric Chemistry and Physics, 6, 5225-5246, 2006.

Schutgens, N. A. J.: Site representativity of AERONET and GAW remotely sensed AOT and AAOT observations, Atmos. Chem. Phys. Discuss., 2019, 1-29, 2019.

Sherwood, S. C., Bony, S., Boucher, O., Bretherton, C., Forster, P. M., Gregory, J. M. and Stevens, B.: Adjustments in the Forcing-Feedback Framework for Understanding Climate Change, Bulletin of the American Meteorological Society, 96(2), 217-228, 2015.

Smith, C. J., Kramer, R. J., Myhre, G., Forster, P. M., Soden, B. J., Andrews, T., Boucher, O., Faluvegi, G., Fläschner, D., Hodnebrog, Ø., Kasoar, M., Kharin, V., Kirkevåg, A., Lamarque, J.-F., Mülmenstädt, J., Olivié, D., Richardson, T., Samset, B. H., Shindell, D., Stier, P., Takemura, T., Voulgarakis, A. and Watson-Parris, D.: Understanding Rapid Adjustments to Diverse Forcing Agents, Geophysical Research Letters, 45(21), 12,023-12,031, 2018.

Stier, P., Schutgens, N. A. J., Bellouin, N., Bian, H., Boucher, O., Chin, M., Ghan, S., Huneeus, N., Kinne, S., Lin, G., Ma, X., Myhre, G., Penner, J. E., Randles, C. A., Samset, B., Schulz, M., Takemura, T., Yu, F., Yu, H. and Zhou, C.: Host model uncertainties in aerosol radiative forcing estimates: results from the AeroCom Prescribed intercomparison study, Atmospheric Chemistry and Physics, 13(6), 3245-3270, 2013.

Takemura, T., Nakajima, T., Dubovik, O., Holben, B. N. and Kinne, S.: Single-scattering albedo and radiative forcing of various aerosol species with a global three-dimensional model, Journal of Climate, 15(4), 333-352, 2002.

Tsigaridis, K., Daskalakis, N., Kanakidou, M., Adams, P. J., Artaxo, P., Bahadur, R., Balkanski, Y., Bauer, S. E., Bellouin, N., Benedetti, A., Bergman, T., Berntsen, T. K., Beukes, J. P., Bian, H., Carslaw, K. S., Chin, M., Curci, G., Diehl, T., Easter, R. C., Ghan, S. J., Gong, S. L., Hodzic, A., Hoyle, C. R., Iversen, T., Jathar, S., Jimenez, J. L., Kaiser, J. W., Kirkevåg, A., Koch, D., Kokkola, H., Lee, Y. H., Lin, G., Liu, X., Luo, G., Ma, X., Mann, G. W., Mihalopoulos, N., Morcrette, J. J., Müller, J. F., Myhre, G., Myriokefalitakis, S., Ng, N. L., O'Donnell, D., Penner, J. E., Pozzoli, L., Pringle, K. J., Russell, L. M., Schulz, M., Sciare, J., Seland, Ø., Shindell, D. T., Sillman, S., Skeie, R. B., Spracklen, D., Stavrakou, T., Steenrod, S. D., Takemura, T., Tiitta, P., Tilmes, S., Tost, H., van Noije, T., van Zyl, P. G., von Salzen, K., Yu, F., Wang, Z., Wang, Z., Zaveri, R. A., Zhang, H., Zhang, K., Zhang, Q. and Zhang, X.: The AeroCom evaluation and intercomparison of organic aerosol in global models, Atmos. Chem. Phys., 14(19), 10845-10895, 2014.

Wang, Q. Q., Jacob, D. J., Spackman, J. R., Perring, A. E., Schwarz, J. P., Moteki, N., Marais, E. A., Ge, C., Wang, J. and Barrett, S. R. H.: Global budget and radiative forcing of black carbon aerosol: Constraints from pole-to-pole (HIPPO) observations across the Pacific, Journal of Geophysical Research-Atmospheres, 119(1), 195-206, 2014.

Wang, R., Andrews, E., Balkanski, Y., Boucher, O., Myhre, G., Samset, B. H., Schulz, M., Schuster, G. L., Valari, M. and Tao, S.: Spatial Representativeness Error in the Ground-Level Observation Networks for Black Carbon Radiation Absorption, Geophysical Research Letters, 45(4), 2106-2114, 2018.

Zhang, Z., Meyer, K., Yu, H., Platnick, S., Colarco, P., Liu, Z. and Oreopoulos, L.: Shortwave direct radiative effects of above-cloud aerosols over global oceans derived from 8 years of CALIOP and MODIS observations, Atmos. Chem. Phys., 16(5), 2877-2900, 2016.

Zuidema, P., Redemann, J., Haywood, J., Wood, R., Piketh, S., Hipondoka, M. and Formenti, P.: Smoke and Clouds above the Southeast Atlantic: Upcoming Field Campaigns Probe Absorbing Aerosol's Impact on Climate, Bulletin of the American Meteorological Society, 97(7), 1131-1135, 2016.

Tables

Table 1. Diagnostics from AeroCom Phase 2 (Myhre et al., 2013a; Samset et al., 2013; Stier et al., 2013) used in multivariate data analysis to investigate factors influencing the contribution of cloudy sky to RFari. The variable "Cloudy" is the contribution of cloudy sky to RFari (second term on the right-hand side of equation 1). FIX2scat and FIX3abs are the contributions from cloudy sky to RFari in two highly idealized aerosol radiative properties experiments in Stier et al. (2013), where FIX2scat is a purely scattering aerosol case and FIX3abs is an absorbing aerosol case. The other variables, from AeroCom phase II model simulations, are total short-wave cloud radiative effect (SW_CRE), cloud fraction (CLD_FR), weighed cloud height (CL_ALT), weighted anthropogenic aerosol height (AER_ALT), single scattering albedo (SSA) of anthropogenic aerosols and fraction of anthropogenic BC mass above 5 km (BC_mass_5km). The variables Cloudy, FIX2scat, FIX3abs and SW_CRE are given in Wm^{-2}, CLD_FR and BC mass>5km in percent, with SSA unitless. AER_ALT and CL_ALT are given in hPa where the pressure levels are weighted by aerosol extinction and cloud fractions, respectively.

		Host model dependences					Aerosol properties		
Models	Cloudy	FIX2scat	FIX3abs	SW_ CRE	CLD FR	CL ALT	AER ALT	SSA	BC mass >5km
	W m-2	W m-2	W m-2	W m-2	%	hPa	hPa	1	%
CAM5	0.121	-1.8	1.8	-48.4	64	592	908	0.901	18.1
GOCART	-0.114	-1.6	1.2	-21.8	58	520	867	0.937	27.1
HadGEM2	0.0554	-1.1	1.5	-53.1	55	638	921	0.947	33.6
IMPACT	0.114	-1.5	2.1	-68.6	66	554	850	0.973	5.8
LMDZ-INCA	0.0756	-0.8	2.5	-53.1	47	585	NA	0.968	28.9
ECHAM-HAM	-0.0242	-1.7	1.1	NA	63	NA	NA	0.936	10.8
OsloCTM2	0.0934	-1.4	1.4	-49.3	62	616	885	0.939	30.1
SPRINTARS	0.155	-1.5	1.7	-47.4	60	525	913	0.958	30.3

Figures

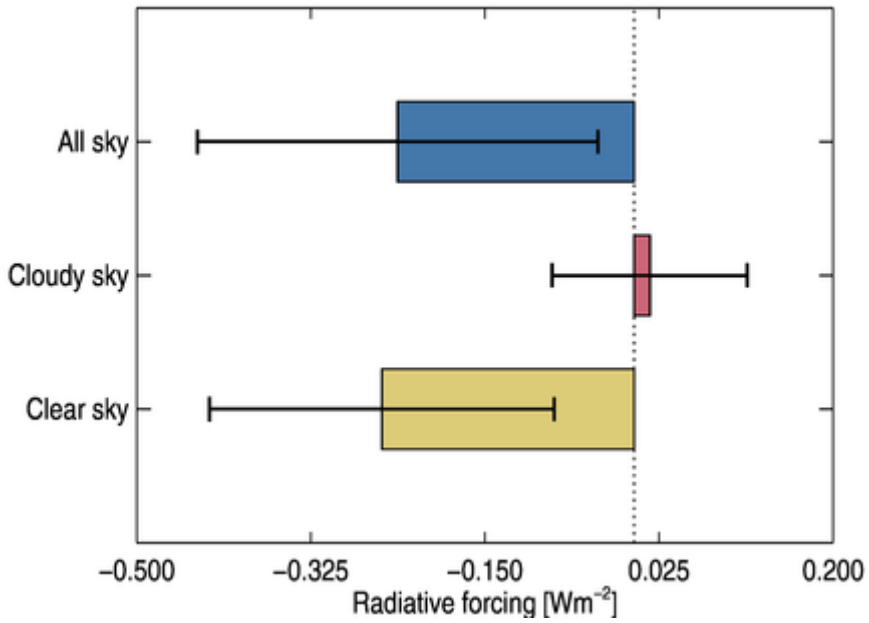

495

Figure 1: All sky anthropogenic RFari, and its decomposition into contributions from cloudy sky and clear sky areas (second and first term on the right hand of equation 1, respectively), based on AeroCom Phase II simulations (Myhre et al., 2013a).

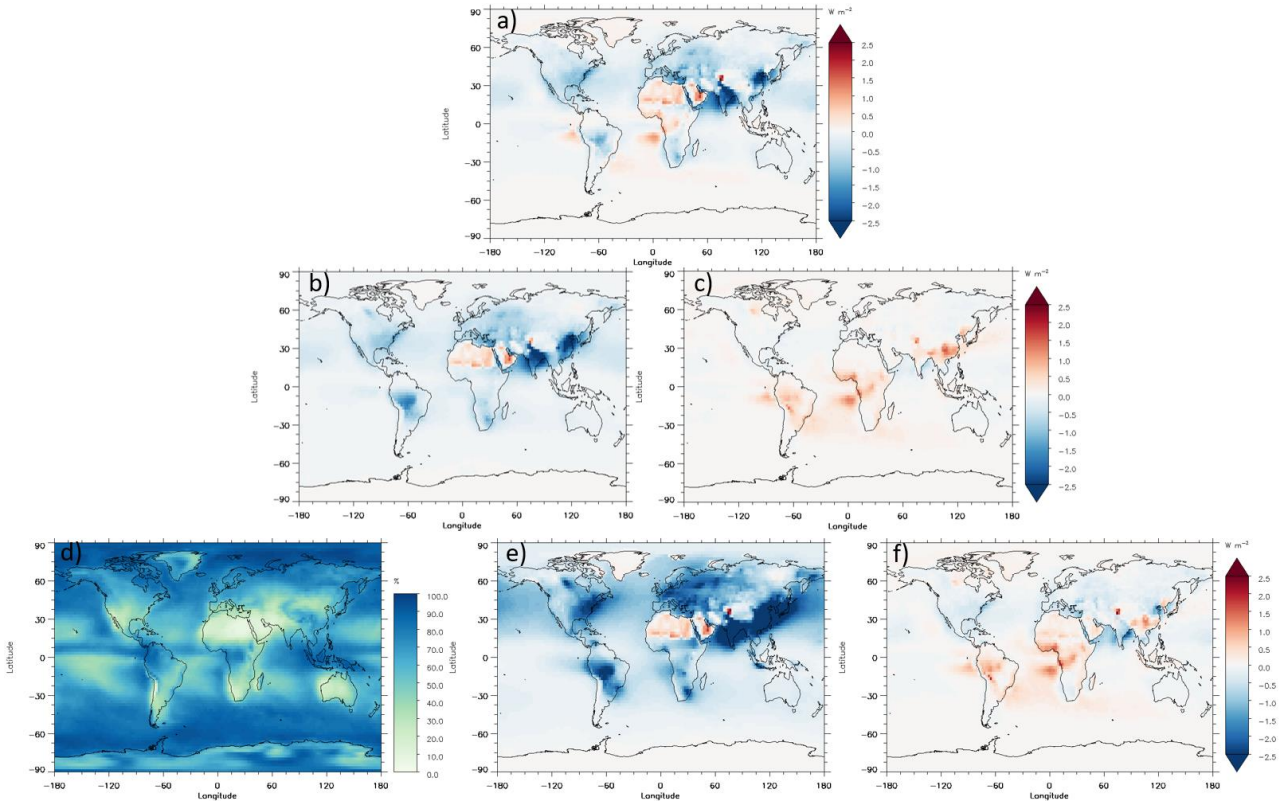

Figure 2. Annual mean all sky anthropogenic RFari and various terms from clear and cloudy skies simulated with OsloCTM3 (Lund et al., 2018). The panel in the top row show the all sky RFari a), the second row shows the contributions from clear ($RFari_{clear}$) and cloudy sky ($RFari_{cloud}$) (first b) and second term c) on right hand side on equation 1, respectively). The third row shows cloud fraction (AC) d), $RFari_{total-clear}$ e) and $RFari_{total-cloud}$, f) respectively. Panel d) on cloud fraction is showed in percent and the other panels in W m^{-2}.

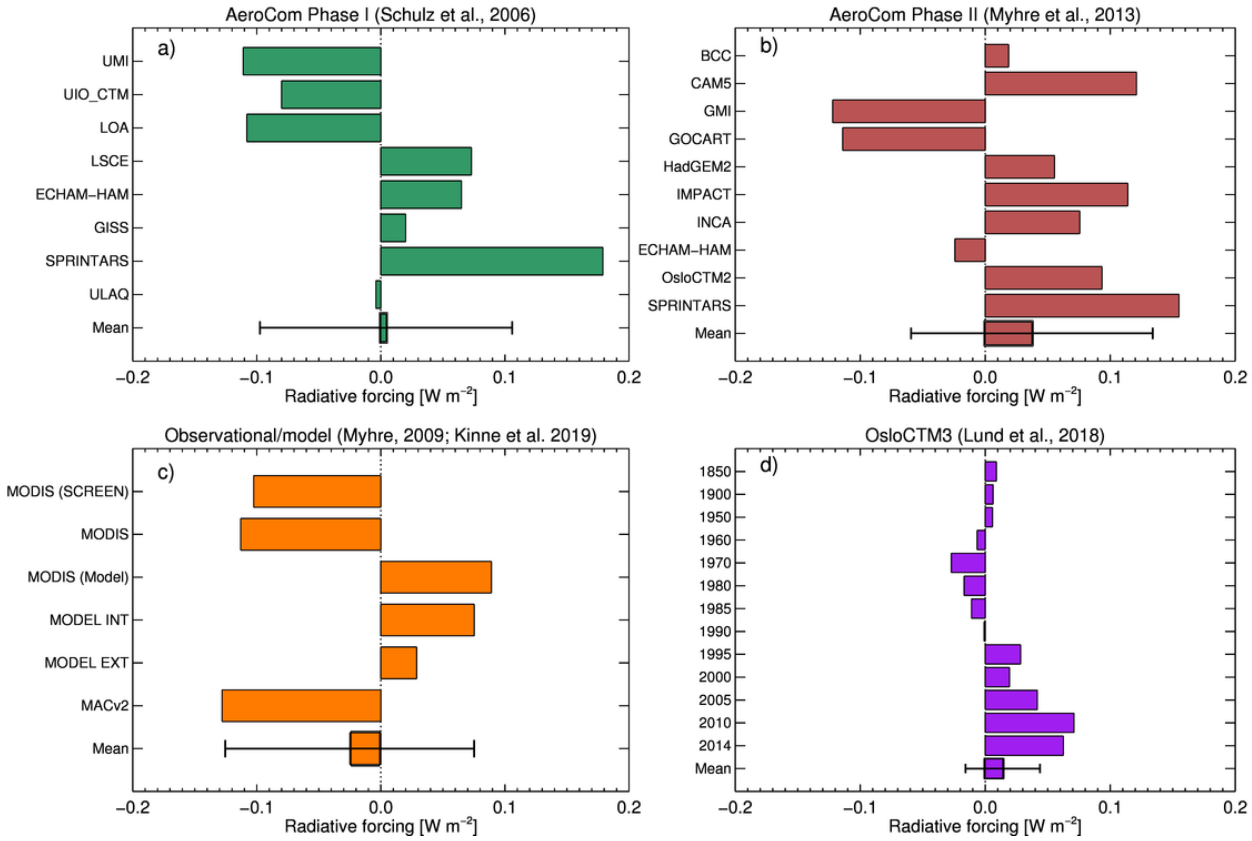

Figure 3. The contribution of cloudy sky to RFari from AeroCom Phase I (Schulz et al., 2006) a), AeroCom Phase II (Myhre et al., 2013a) b), combination of observational based and model simulation (Kinne, 2019a; Myhre, 2009), where mean and standard deviation are based on all methods used in the panel c), and time evolution from OsloCTM3 (Lund et al., 2018) d).The multi-model mean is shown by the bars and the one standard uncertainty range of the models is given by whiskers.

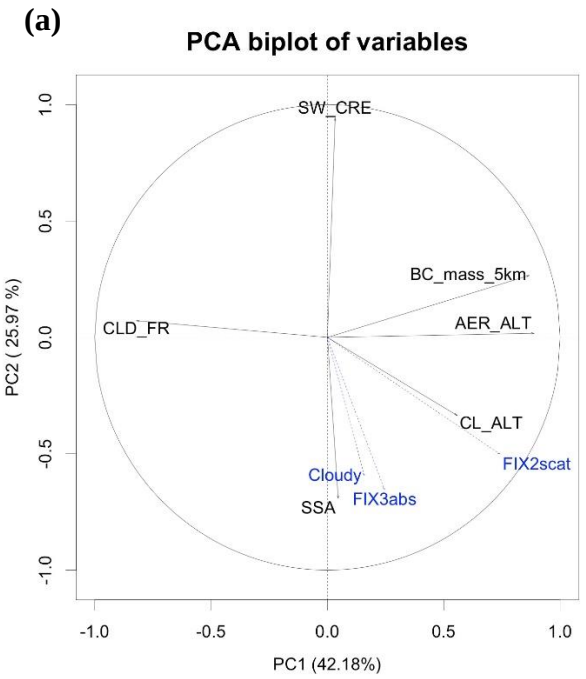
(a)
PCA biplot of variables
SW_CRE
BC_mass_5km
CLD_FR
AER_ALT
CL_ALT
FIX2scat
Cloudy
FIX3abs
SSA
PC2 (25.97 %)
PC1 (42.18%)
1.0
0.5
0.0
-0.5
-1.0

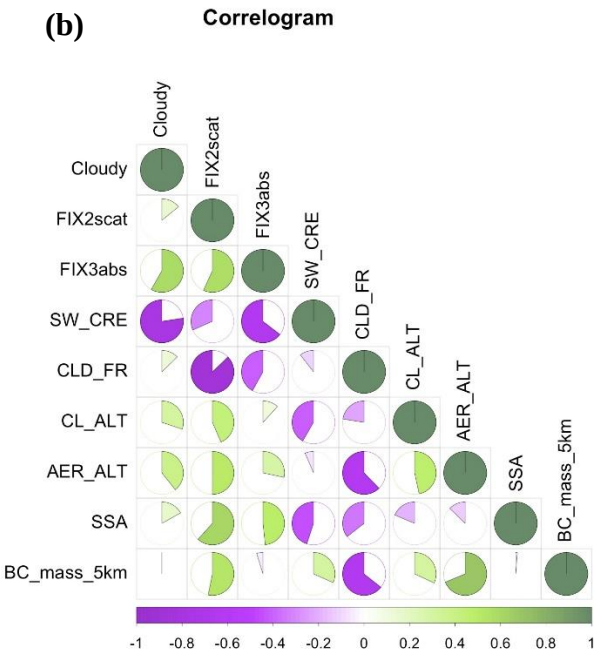
(b)
Correlogram
Cloudy
FIX2scat
FIX3abs
SW_CRE
CLD_FR
CL_ALT
AER_ALT
SSA
BC_mass_5km
-1
-0.8
-0.6
-0.4
-0.2
0
0.2
0.4
0.6
0.8
1

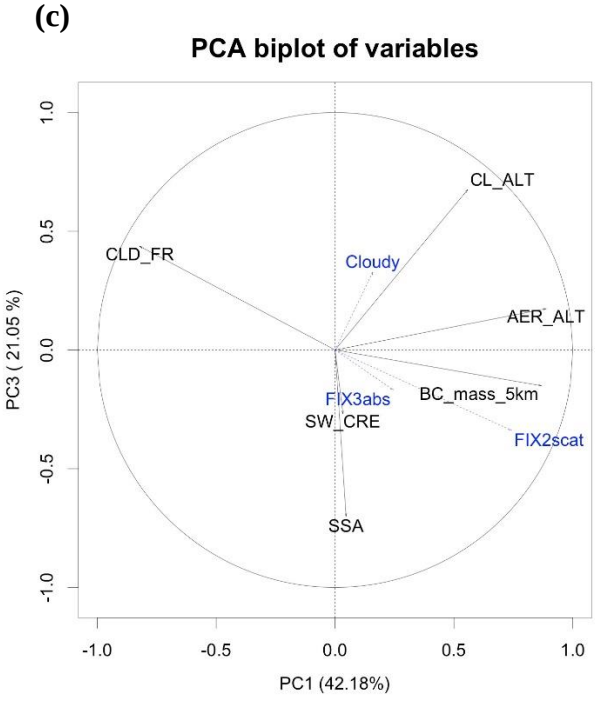
(c)
PCA biplot of variables
CL_ALT
CLD_FR
Cloudy
AER_ALT
FIX3abs
BC_mass_5km
SW_CRE
FIX2scat
SSA
PC3 (21.05 %)
PC1 (42.18%)
1.0
0.5
0.0
-0.5
-1.0

515

Figure 4. Multivariate data analysis of eight AeroCom Phase II models (Myhre et al., 2013a) using diagnostics shown in Table S1. Principal Component Analysis biplot of the variables a). The length of the arrows indicates the strength of the correlation each variable has in relation to PC1 and PC2, representing 42.2% and 26.0% of the variance respectively. Variables clustered together indicate positive correlation with each other. Variable opposing each other indicate negative correlation. Cloudy, FIX3abs and FIX2scat (in blue) are added as supplementary variables, and do not influence the projection of the other variables. This requirement is made since cloudy, FIX2scat and FIX3abs already depends on the other variable and see their correlation. FIX2scat and FIX3abs have fixed SSA globally and for all models, where the former experiment has pure scattering aerosol and FIX3abs has relatively low SSA (and thus high aerosol absorption). In (b), the correlogram shows the one to one linear regression correlation each variable has to each other. The correlation coefficients (r) are presented on a color scale from -1 (purple) to 0 (white) to +1 (green). The strength of the correlation is additionally presented as pie charts filling clockwise in green for positive correlations between two variables, and counter clockwise in purple for negative correlation, where they can range from empty and full pie charts, indicating an absolute correlation respectively from 0 to 1. Panel (c) is same as for (a), but for PC1 and PC3.